Chapter 6: Simulation Investigations of Second Harmonic Submillimeter-Wave Gyrotron

6.1. Introduction ..... **Error! Bookmark not defined.**

6.2. Modelling of Gyrotron 134

6.2.1 Magnetron Injection Gun ..... **Error! Bookmark not defined.**

6.2.2 Cavity Field Profile 135

6.2.3 Coupling Coefficient and Start Oscillation Current 136

6.3. Multimode Simulation of Submillimeter-Wave Gyrotron 137

6.4. Thermal and Static Structural Analysis 138

6.5. Tuneability of Submillimeter-Wave Gyrotron 141

6.5.1 Magnetic Tuning Scheme 141

6.5.2 Thermal Tuning Scheme 143

6.6. Output System 146

6.6.1 RF Window 146

6.6.2 Output Collector 146

6.7. Conclusion 148

6.1 Introduction

In the preceding chapters, the tuneability of millimeter-wave gyrotrons have been studied at 260 GHz for 400 MHz Nuclear Magnetic Resonance (NMR) spectroscopy applications using both PIC and Multimode simulations. Both the magnetic and thermal tuning schemes have been used to obtain the tuneable bandwidth of those gyrotrons. To observe the effect of ohmic loss, thermal and structural analyses have also been performed.

As explained in Chapter – 1, the resolution in an NMR experiment can be increased by increasing the NMR magnetic field. The DNP technique requires a higher frequency microwave source to increase the signal intensity in the NMR experiment. During the first decade of 21st century, gyrotrons have been successfully demonstrated at 140 GHz, 250 GHz, 260 GHz, 330 GHz, 395 GHz, 460 GHz, 527 GHz, and 670 GHz in various laboratories around the world [59] – [68]. In order to achieve impressive achievements in DNP-NMR applications, a series of higher harmonic THz gyrotrons are successfully being demonstrated in various organizations in the USA [70]–[74], Russia [75] and Japan [76]–[78].

In the present chapter, a submillimeter-wave gyrotron has been investigated at 527 GHz for 800 MHz NMR spectroscopy applications. The beam-wave interaction behavior of the gyrotron has been investigated by using a time-dependent Multimode code. Magnetron Injection Gun (MIG) has been designed using the E-GUN simulation tool. The magnetic tuning scheme has been used to obtain the tuneable bandwidth of the present 527 GHz gyrotron. The design and optimization of the MIG are discussed in section 6.2. Modeling and Multimode simulations of the gyrotron cavity are introduced in section 6.3. Thermal issues of the gyrotron cavity are discussed briefly in section 6.4. Further, the tuneability of the present submillimeter wave gyrotron is discussed in

section 6.5 and the output system including RF window and depressed collector are discussed in section 6.6. Finally, the chapter is concluded in section 6.7.

Table 6.1: Design Parameters of 527 GHz Gyrotron

Parameters	Value
Beam voltage (V_b)	16.75 kV
Anode voltage (V_a)	5.5 kV
Beam current	90 mA
Mean diameter of the cathode	~10 mm
Cathode slant angle	30^0
Guiding center radius	~0.98 mm
Beam thickness ($2*r_L$)	0.04 mm
Compression ratio (F_m)	25
Magnetic Field at Cathode (B_c)	0.35 T
Optimized velocity ratio	~1.8
Transverse velocity spread $(\Delta v_t / v_t)\%$	~ 3 %
Frequency	527.15 – 527.49 GHz
Pitch factor	~1.8
Magnetic field	9.7 T – 9.75 T
Output Power	≥ 1.5 W

6.2 Modeling of Submillimeter-Wave Gyrotron

6.2.1 Magnetron Injection Gun

Magnetron Injection Gun (MIG) is an energy source of gyrotrons to produce an annular electron beam, which is operated in limited temperature regions [139]. The initial design parameters of the triode type MIG are estimated by using a set of adiabatic trade-off equations [140] – [141]. The MIG is designed using an E-GUN simulation tool that provides an extra parametric space like the anode to achieve the desired annular electron beam. The cathode is simulated to achieve the desired guiding center radius, beam thickness, transverse velocity ratio, and velocity spread. The distance between the cathode to anode and the magnetic field profile is optimized to obtain the electron beam profile [Figure 6.1]. The design parameters of the MIG are listed in Table – 6.1. The cathode slant angle (30^0) and shape of the anode are optimized to achieve the velocity

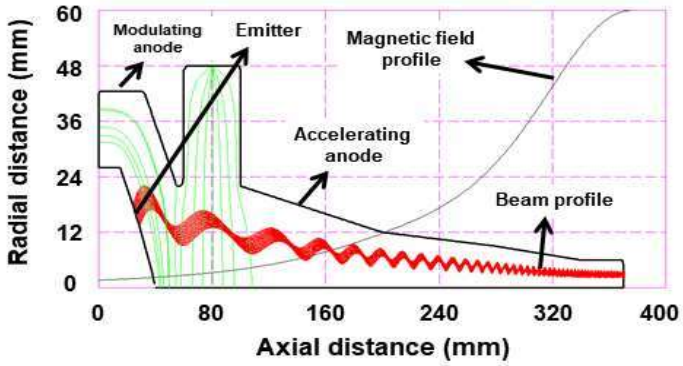

Figure 6.1 Model of MIG with electron beam profile and magnetic field profile.

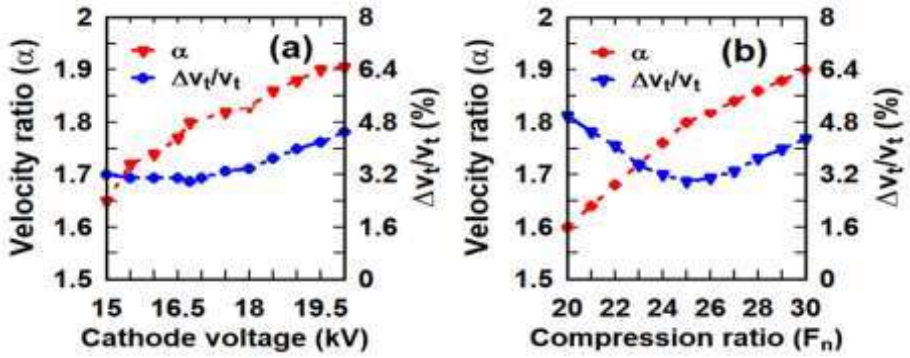

Figure 6.2 Velocity ratio (α) and velocity spread $(\Delta v_t/v_t)\%$ with respect to (a) modulating cathode voltage and (b) compression ratio (F_m).

ratio (α) ~1.8 and velocity spread ~ 3%, for the cathode voltage of 16.75 kV [Figure 6.2 (a)], the compression ratio of ~25 [Figure 6.2 (b)].

6.2.2 Modeling of RF Interaction Cavity

The present sub-millimeter-wave gyrotron cavity modeling is based on the experimentally tested gyrotron by Jawla *et al.* [70]. The initial design of the cavity is

Table 6.2: Structural Parameters of 527 GHz Gyrotron [70]

Structural Parameters	Down taper	Length (mm)	5
		Angle	1.2°
	RF section	Length (mm)	25
		Radius (mm)	1.593
	UP Taper (1)	Length (mm)	10
		Angle	0.3°
	UP Taper (2)	Length (mm)	20
		Angle	0.6°
	UP Taper (3)	Length (mm)	18
		Angle	1.9°

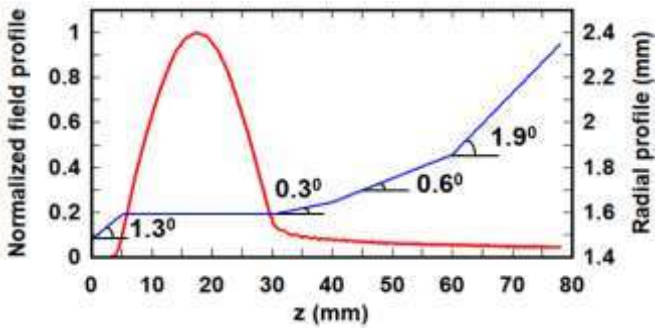

Figure 6.3 Normalized cavity field profile and radial profile of the cavity.

optimized for an axial mode number, q = 1. In the present study, $TE_{11,2,1}$ mode is chosen because it has sufficient frequency separation from the nearby modes such as $TE_{5,4,1}$ to ~8.61 GHz and $TE_{8,3,1}$ to ~5.21 GHz. This frequency separation allows $TE_{11,2,1}$ is a very appropriate mode for the tuneable gyrotron. Generally, the gyrotron cavity consists of three sections: a down taper, straight (interaction) section, and an uptaper. The cavity field profile of the cavity is plotted [Figure 6.3], which shows the maximum intensity of the E–field in the middle of the straight section of the cavity [1]. All the optimized structural parameters are listed in Table – 6.2 [70].

6.2.3 Coupling Coefficient and Start Oscillation Current

The coupling coefficient of co-rotating and counter-rotating $TE_{11,2}$ mode and other nearby modes are plotted as shown in Figure 6.4 (a). The (+) sign stands for co-rotating and (–) sign stands for counter-rotating modes. The guiding center radius is chosen as ~ 0.98 mm, at which the coupling of the electron beam with the co-rotating mode $TE_{11,2}^{+}$ is maximum. The coupling of the electron beam with the operating $TE_{11,2}$ mode has a significant separation from the coupling of the electron beam with the other competing co-rotating $TE_{5,4}^{+}$, $TE_{8,3}^{+}$ and counter-rotating $TE_{8,3}^{-}$, $TE_{3,5}^{-}$ modes, as shown in Figure 6.4 (a). The start oscillation current (SOC) [102] of these modes are plotted by using the linear theory for axial mode number q = 1, as shown in Figure 6.4 (b). The minimum SOC of co-rotating $TE_{11,2,1}$ mode is calculated as ~21 mA. The SOC of co-

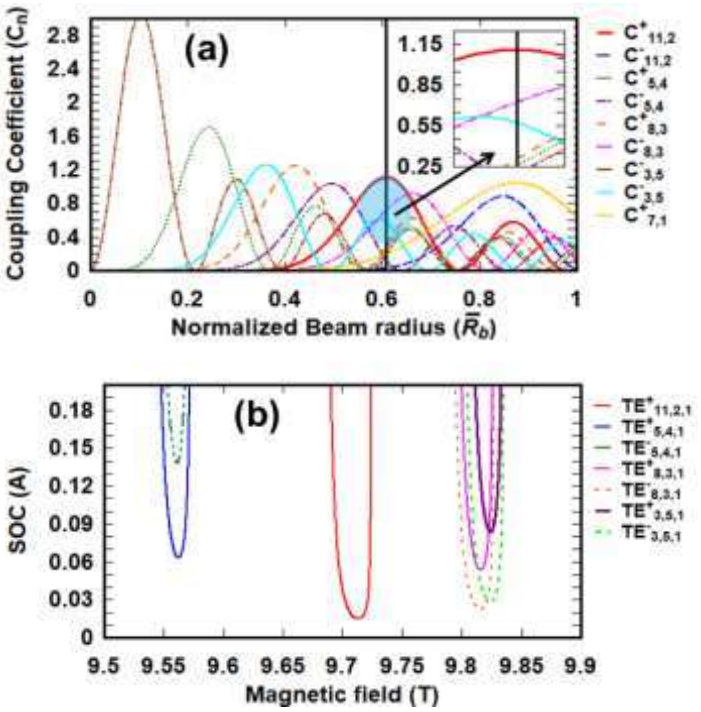

Figure 6.4 (a) Coupling coefficient and (b) start oscillation current of $TE_{11,2,1}$ mode along with other competing modes.

rotating $TE_{11,2,1}$ mode has enough separation from its nearby competing modes such as $TE^{-}_{8,3}$, $TE^{-}_{3,5}$, $TE^{+}_{5,4}$, and $TE^{+}_{8,3}$, which is sufficient to excite a series of axial modes of $TE^{+}_{11,2,q}$ for frequency tuning of the cavity, where 'q' is the axial index number.

6.3 Multimode Simulation of Submillimeter-Wave Gyrotron

A self-consistent non-linear time-dependent Multimode theory [91] has been used to investigate the growth of power in the operating co-rotating $TE_{11,2,1}$ mode and co-rotating and counter-rotating $TE_{5,4}$, $TE_{8,3,}$ and $TE_{3,5}$ modes. The present Multimode simulation is run for 500 ns with 2 ps time steps. A total of 32 beamlets are considered with 32 electrons in each beamlets in the Multimode simulation. The parameters used in the present simulation including guiding center radius, Larmor radius, beam voltage, beam current, velocity ratio and velocity spread are listed in Table – 6.1. The beam parameters are considered as V_b = 16.75 kV, I_b = 90 mA, B_o = 9.70 T and $\alpha \cong 1.8$, and

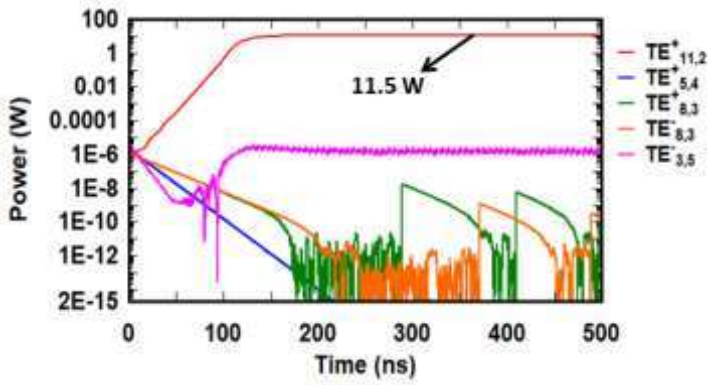

Figure 6.5 Output power in operating $TE_{11,2}$ mode along with competing modes.

~3 % velocity spread in the Multimode simulation. In addition to the operating $TE^{+}_{11,2}$ mode, the other competing modes such as $TE^{+}_{8,3}$, $TE^{-}_{8,3}$, $TE^{+}_{5,4}$ and $TE^{-}_{3,5}$ are also considered in the Multimode simulations. The present Multimode simulation predicted ~11.5 W of the saturated power in the $TE_{11,2}$ mode at ~527.20 GHz. It is clear from Figure 6.5 that almost negligible power is observed in competing $TE^{+}_{8,3}$, $TE^{-}_{8,3}$, $TE^{+}_{5,4}$ and $TE^{-}_{3,5}$ modes.

6.4 Thermal and Static Structural Analysis

The present RF cavity is modeled in a finite element method (FEM) based commercially available ANSYS [113], to observe its thermal and structural characteristics. The Oxygen-Free High Conductivity Copper (OFHC-Cu) is used to model the cavity with reduced conductivity, $\sigma = \sigma_{Cu}/2 = 2.9 \times 10^{7}$ S/ m. Other properties of the OFHC-Cu are remained same as used in 260 GHz gyrotron design discussed in Chapter – 3. The skin depth (δ) is calculated as ~1.288×10^{-7} m at the resonating frequency of ~527.20 GHz. As the main beam-wave interaction is taking place in the straight section of the RF interaction circuit, where the ohmic loss (wall loss) is maximum. The ohmic loss is calculated as ~0.062 kW /cm^2 [109], [114] for the output power ~12 W and the diffractive quality factor (Q_d) is calculated as ~97000. The ohmic

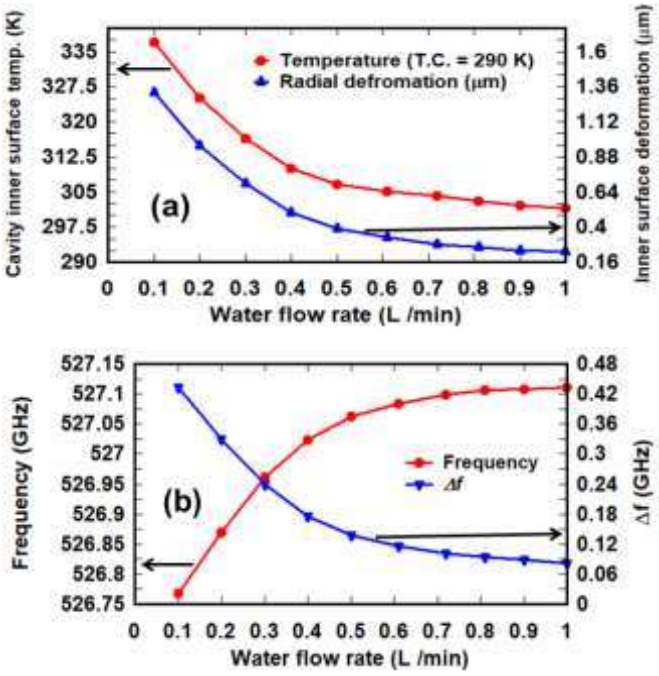

Figure 6.6 (a) Cavity inner surface temperature and inner surface temperature with respective water flow rate and (b) resonant frequency, and shifting in resonating frequency of the cavity with respective water flow rate.

loss of the cavity is treated as heat flux in the simulation, which is applied at the inner surface of the straight section of the interaction circuit. The thickness of the cavity is considered as 2 mm. To cool down the cavity, radial grooves are used at the outer surface of the cavity. The thickness and height of grooves are optimized as 1 mm and 2 mm, respectively. The spacing between the grooves is optimized as 2 mm. A total of 10 grooves have been used on the RF interaction cavity surface in the simulation. To observe the temperature distribution and deformation of the cavity, the Fluent Solver and Static Structural Solver are used, respectively. In the present simulation, Water is used as a coolant that flows between the grooves at the cavity's outer surface. The conductivity and Prandtl number (P_r) of water are considered as 0.6 W /m – K and 6.99, respectively. 3D steady-state and absolute velocity formulations are used in the Fluent simulation of ANSYS. The κ–ε turbulence model with enhanced wall treatment is chosen for estimating the pressure gradient near the water-copper wall regions. The fine

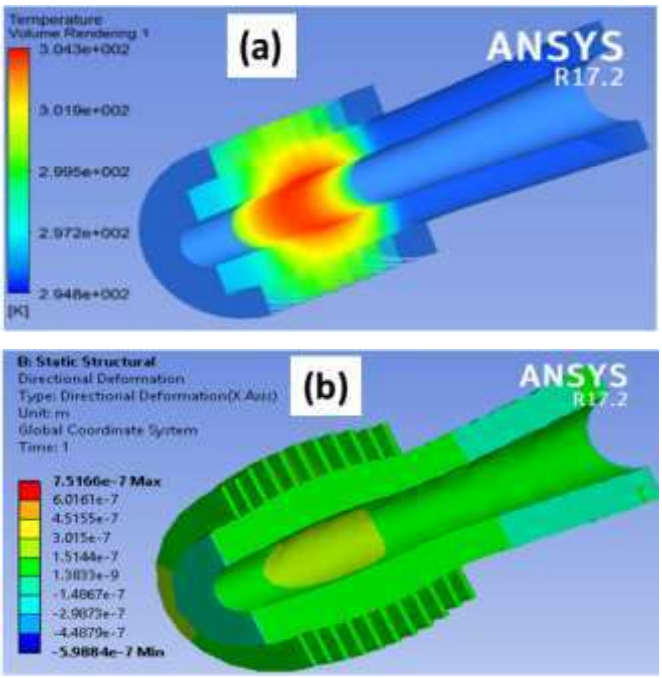

Figure 6.7 (a) Temperature distribution of the cavity, (b) deformation distribution of the cavity with the coolant (water) temperature 290 K, and 0.7 L /m fluid flow between the grooves.

meshing is used in the simulation with 35,745 nodes having 20,325 elements. In the present thermal studies, the wall boundary-loaded heat flux distribution on the cavity's inner surface is chosen as the boundary condition. The velocity–inlet for the inlet surface, pressure-outlet for the outlet surface are considered in the simulation and the default boundaries are selected for other surfaces. The average surface heat transfer coefficient is calculated using the post-processing of the simulation. The water flow rate is optimized as 0.7 L /min through a single groove because when the coolant flow rate is beyond this, a continuum in temperature and deformation is found, as shown in Figure 6.6 (a). The thermal deformation is affected by the resonant frequency of the RF interaction cavity. Since thermal distortion is dependent on the coolant flow rate at the outer surface of the RF interaction cavity, the resonant frequency (f_r) and the shift in resonating frequency (Δf_r) [Figure 6.6 (b)] of the cavity are calculated with respective water flow rate. The Figure 6.6 (b) shows that at the flow rates above 0.7 L / min of water, both the resonant frequency and the change in the resonant frequency are almost

constant. The maximum temperature is observed as ~311 K in the middle of the cavity [Figure 6.7 (a)] at the coolant temperature (T.C.) of 290 K. The maximum pressure at the inlet surface and minimum pressure at the outlet surface are calculated as ~1.39 $\times 10^4$ Pa and ~2.04 $\times 10^2$ Pa, respectively. The deformation of the cavity is observed by importing both the calculated temperature and pressure as a load in the Static Structural Solver. Both ends of the cavity are fixed in the simulation to observe the radial deformation by considering the temperature and pressure on the cavity individually. It is observed that the deformation due to temperature (~10^{-6} m) is found ~10^4 times higher than the deformation due to the pressure of water (~10^{-10} m) on the cavity. The resonating frequency is sensitive to the radius of the straight section of the cavity, which is shifted with the deformation of the cavity. The average deformation [Figure 6.7 (b)] at the inner surface of the straight section of the cavity is observed as ~0.28 μm at a water temperature of 290 K. At this deformation, the resonant frequency of the RF cavity is observed as ~527.10 GHz by using the Eigenmode Solver of the CST Microwave Studio. The average temperature at the cavity's inner surface is observed as only ~295 K with the coolant temperature 280 K. At this coolant temperature, no deformation is observed in the cavity and resonated at ~527.20 GHz. Thus, the resonating frequency is shifted by ~0.1 GHz and this shift in resonating frequency is enhanced the tuneable bandwidth of the gyrotron.

6.5 Tuneability of Submillimeter-Wave Gyrotron

6.5.1 Magnetic Tuning Scheme

The start oscillation current (SOC) of various axial number (q) of the desired operating mode is depending upon the applied magnetic field, as shown in Figure 6.8. Therefore, a series of higher-order axial modes of $TE_{11,2,q}$ can be excited in the cavity by varying

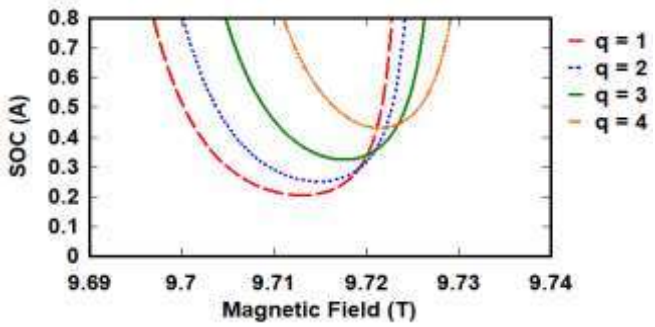

Figure 6.8 SOC of the $TE_{11,2,q}$ mode with axial mode number q = 1 – 4.

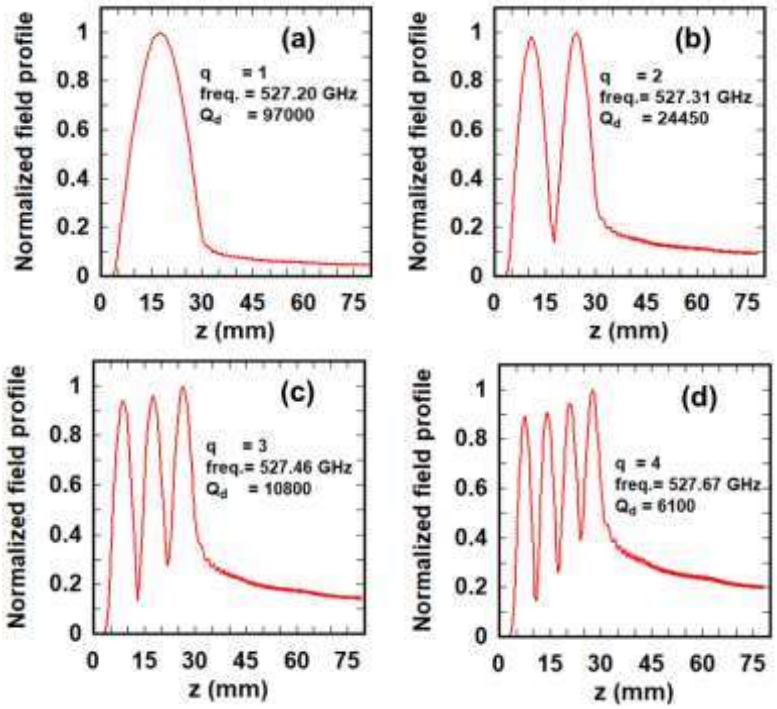

Figure 6.9 The cavity field profile for axial mode number q = 1 – 4.

the magnetic field. The diffractive quality factor (Q_d) of the higher-order axial mode number is reduced abruptly by ~1 /q^2, as shown in Figures 6.9 (a) – 6.9 (d). As a result, the output power in higher-order mode is also reduced but at the same time, the resonating frequency of the gyrotron is pushed up. In the present case, the magnetic tuning is achieved by varying the magnetic field in the span of 9.7 T – 9.75 T and the output power is observed for more than ~1.5 W [Figure 6.10 (a)], by keeping the

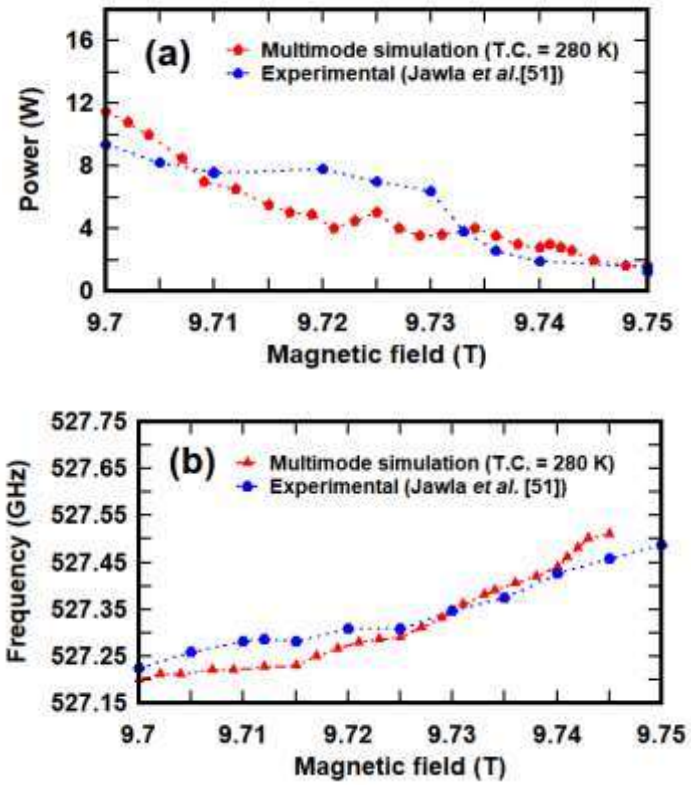

Figure 6.10 (a) Power Vs magnetic field (b) resonating frequency with respective magnetic field (beam parameters are 16.75 kV, 90 mA, α = 1.8, and total velocity spread is 3%).

coolant temperature as ~280 K. The frequency tuning is achieved as ~0.31 GHz [Figure 6.10 (b)] while the RF output power is maintained for more than ~1.5 W in the frequency span of 527.20 GHz –527.51GHz, as the axial mode number (q) is varied from 1 to 3 only. For the axial mode number q = 4, the RF output power is found negligible. The present theoretical results are found to be in close agreement with an experimental gyrotron [70], as shown in Figure 6.10 (a) and 6.10 (b).

6.5.2. Thermal Tuning Scheme

Thermal tuning is another technique to enhance the tunable bandwidth of gyrotron by controlling the cavity's thermal deformation. In this technique, the shift in the resonant frequency of the RF cavity is controlled by varying the coolant temperature at its outer surface. The thermal tuning has an advantage over the magnetic

Table 6.3: Comparison of Deformation Obtained by ANSYS and Theory

Coolant Temp.	Temp. at Inner Surface	ΔR at Inner Surface [ANSYS]	ΔR at Inner Surface [Theoretical]	Difference (%)
290 K	304.1 K	0.28 μm	0.298 μm	6.4
310 K	324.5 K	0.92 μm	0.84 μm	8.7
330 K	344.2 K	1.52 μm	1.381 μm	9.7
350 K	364.3 K	2.2 μm	1.923 μm	12.6

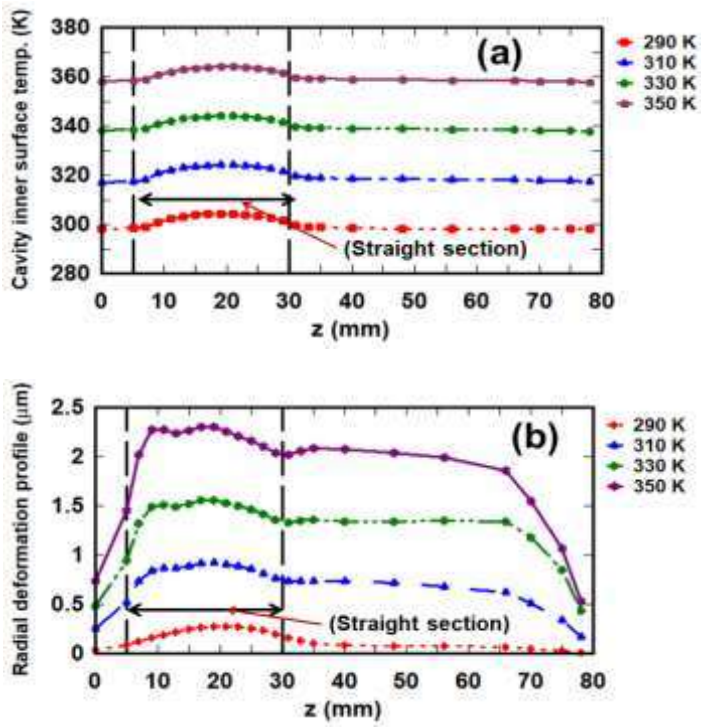

Figure 6.11 (a) Temperature distribution and (b) deformation distribution at the inner surface of the cavity for different coolant temperatures along the axial length of the cavity.

tuning is that it has a higher efficiency (power), because the device is operated in the desired mode with the fundamental axial mode number, *i.e.* $q = 1$. In the present case, the thermal tuning is performed by varying the coolant temperature from 290 K to 350 K at the outer surface of the cavity. The temperature at the inner surface of the straight section of RF cavity is observed as ~304.10 K, ~324.5 K, ~344.2 K and ~364.3 K corresponding to the coolant (water) temperature of 290 K, 310 K, 330 K, and 350 K, respectively, as shown in Figure 6.11 (a). The deformation at the inner surface of RF interaction circuit is estimated as ~0.28 μm, ~0.92 μm, ~1.53 μm and ~2.2 μm

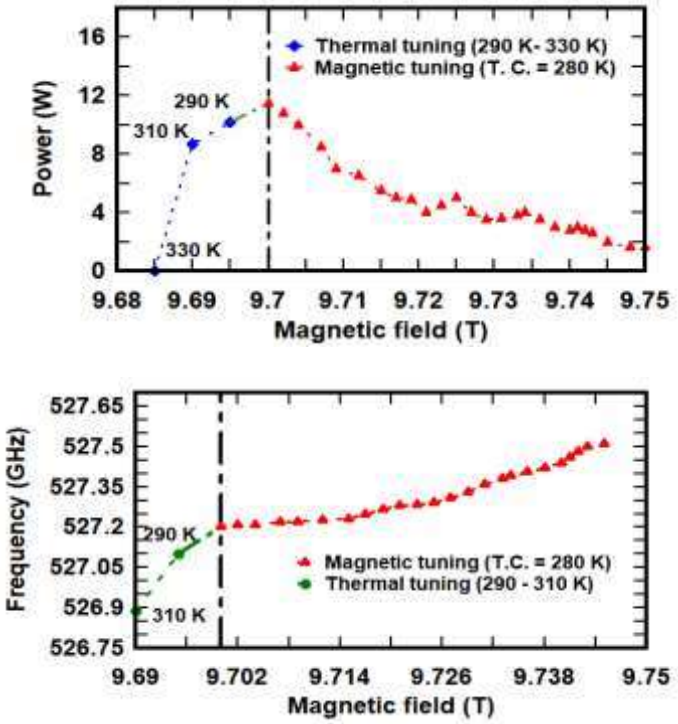

Figure 6.12 (a) Power and (b) resonant frequency with respect to B-field for both thermal and magnetic tuning schemes.

corresponding to the coolant temperature of 290 K, 310 K, 330 K, and 350 K, respectively, as shown in Figure 6.11 (b). The obtained deformation from the Static Structural Solver has shown a good agreement with the theoretically obtained deformation corresponding to the cavity temperature, as listed in Table – 6.3. The deformation in the cavity is theoretically estimated by using $\Delta R = R_c * \alpha * \Delta T$, where, R_c is the cavity radius, α (17 μm /^{o}C) is the thermal expansion coefficient and ΔT is the rise in temperature from the room temperature ~293 K. The resonant frequency of the present gyrotron cavity is calculated using Eigenmode Solver of 'CST Microwave Studio'. The cavity's resonant frequency is observed as ~527.10 GHz, ~526.89 GHz, ~526.68 GHz, and ~526.43 GHz corresponding to the coolant temperature of 290 K, 310 K, 330 K, and 350 K, respectively. Therefore, the corresponding shift in resonating frequencies (Δf) is ~0.1 GHz, ~0.31 GHz, ~0.52 GHz, and ~0.74 GHz, respectively. The Multimode simulation of the present gyrotron predicted and RF output power [Figure

6.12 (a)] of ~12.2 W and ~11.5 W for an optimized magnetic field of 9.695 T and 9.69 T, at ~527.10 GHz and ~526.89 GHz [Figure 6.12 (b)] corresponding to the coolant temperature of 290 K and 310 K, respectively. A negligible amount of power is observed at a higher coolant temperature of 330 K and 350 K. Therefore, the tuneable frequency is enhanced as ~0.31 GHz by the thermal tuning scheme individually with respect to the obtained resonant frequency ~527.20 GHz at the coolant temperature of 280 K.

6.6 Output System

6.6.1. RF Window

The output window plays a crucial role in the gyrotron oscillator, which couples the RF wave to the external system and isolates the vacuum inside the gyrotron. In the present case, a single disk window is designed by using Fused Quartz [$\varepsilon_r = 3.78$, $\tan(\delta) = 6 \times 10^{-5}$] having a thickness of 3.365 mm and diameter of ~42 mm. The absorption coefficient (A_b) [118] is calculated as 0.5 % at 527.20 GHz for $TE_{11,2,1}$ mode. The transmission coefficient (S_{21}) and reflection coefficient (S_{11}) are calculated as –0.023 dB and –53.45 dB at ~527.20 GHz for $TE_{11,2,1}$ mode, respectively [Figure 6.13]. It is observed that the window is more transparent for $TE_{11,2,q}$ modes (for q = 1 – 3) in the frequency spectrum of ~526.86 GHz to ~527.50 GHz, as compared to other competing modes $TE_{5,4,1}$ and $TE_{8,3,1}$ at ~518.65 GHz and ~532.37 GHz, respectively.

6.6.2. Output Collector

The efficiency of the DNP / NMR gyrotron is very low, which indicates that a very small amount of available electron beam energy is transferred to the RF wave, while a large amount of the remaining electron beam energy is collected at the collector wall which is dissipated as heat power. In the present study, a single-stage depressed

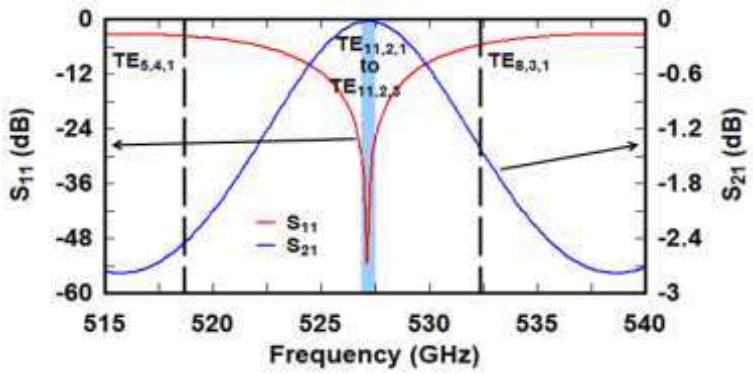

Figure 6.13 Transmission and reflection characteristics of the single disk Fused Quartz window at $\varepsilon_r = 3.78$, $\tan(\delta) = 6 \times 10^{-5}$.

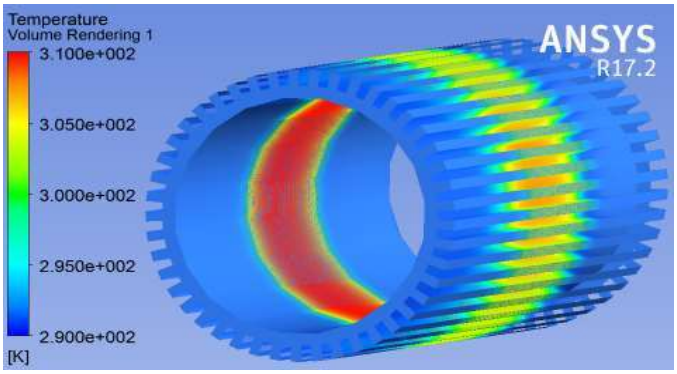

Figure 6.14 Temperature distribution of the collector.

collector has been proposed with the assumption of a thermal loading limit of < 0.5 kW / cm^2 [37] to collect the spent electron beam. The amount of external magnetic field is drastically reduced, *i.e.* ~0.01 T in the collector section. This reduced magnetic field disperses the electron beam in such a way that the probability of secondary electron emission is reduced to a large extent. In general, the electron beam radius in the collector region [1] is approximately equal to the collector radius. Therefore, the radius of the collector has been estimated to be ~30 mm after calculating the electron beam radius in the collector region. In the collector region, the axial beam's width [119] is approximately equal to two times the Larmor radius of the beam present there. The Larmor radius of the beam in the collector region is calculated as ~ 45 mm so the width of the axial beam becomes ~ 90 mm, as a result, the surface area for the heat load in the

collector area is calculated as ~ 169.56 cm^2 ($2\pi \times 30 \times 90\ mm^2$). For the worst-case (*i.e.,* when no energy is recovered in the collector region), the heat load is calculated as ~9.8 W /cm^2. The total length of collector is calculated as ~270 mm, which is thrice of the axial beam width so that the collector collects the unused electron beam at the center. The highest temperature of the ~310 K [Figure 6.14] is observed at the collector's inner surface when the water flow rate of 0.7 L /min in the groove is maintained. Therefore, deformation in the collector region is negligible and is the most desirable condition for its operation.

6.7 Conclusion

A submillimeter-wave gyrotron has been modeled to operate in $TE_{11,2,q}$ mode at ~527 GHz for DNP / NMR applications. The Multimode simulation of gyrotron has predicted ~11.5 W power in the operating $TE_{11,2,1}$ mode at 527.20 GHz. The thermal analysis has been performed to observe ohmic loss's effect in the cavity by using the Fluent Solver in ANSYS. The deformation behavior of the cavity was observed by using the Static Structural solver. The tuneable bandwidth has been achieved as ~0.31 GHz in the magnetic tuning by varying magnetic fields in the span of 9.7 T – 9.75 T. Further, the tuneable bandwidth has been enhanced by using thermal tuning scheme as ~0.30 GHz. Since both tuning schemes are independent, the tuning bandwidths obtained from both schemes are added to have a total tunable bandwidth of gyrotron as ~0.61 GHz (~0.31 GHz by magnetic tuning and ~0.30 GHz by thermal tuning scheme). Therefore, the tuneable bandwidth has been enhanced by ~49 % using thermal tuning schemes.